



Synthesis of Ilmenite NiTiO₃ Rods and Effect of pH on Rhodamine B Textile Dye Degradation under LED Visible-Light Irradiation

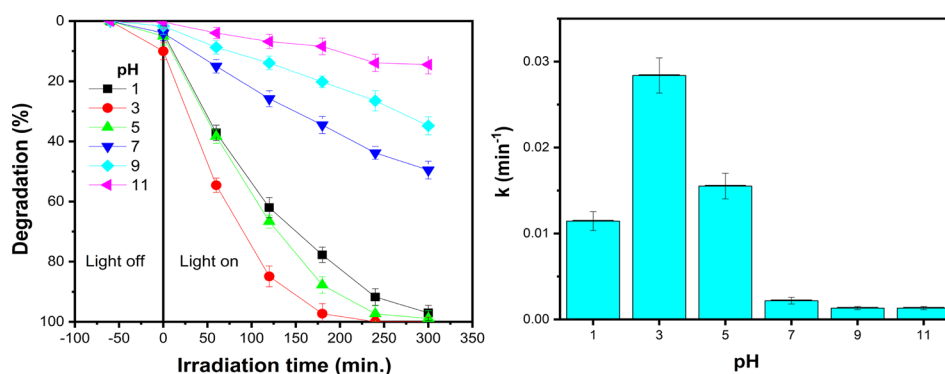
Nguyen Thi Thu Trang¹ · Do Manh Khang¹ · Dang Duc Dung¹ · Nguyen Ngoc Trung¹ · Nguyen Thanh Phuong¹ · Luong Huu Bac¹

Received: 4 July 2021 / Accepted: 27 September 2021 / Published online: 12 October 2021
© The Minerals, Metals & Materials Society 2021

Abstract

NiTiO₃ rods have been synthesized and the influence of pH on their photocatalytic activity under light-emitting diode (LED) irradiation investigated. Ilmenite NiTiO₃ rods were synthesized by an ethylene glycol-mediated route at room temperature, followed by calcination in air. The samples were characterized using x-ray diffraction analysis, scanning electron microscopy, ultraviolet–visible (UV–Vis) spectroscopy, and photocatalytic methods. Photocatalytic degradation of rhodamine B was carried out using NiTiO₃ rods under LED visible-light irradiation. The synthesized NiTiO₃ rods were in pure rhombohedral phase after calcination at 600°C for 2 h. The rods were formed from small nanoparticles of about 30 nm with porous structure. The NiTiO₃ rods presented a visible absorbance response and could degrade RhB dye under visible-light irradiation. The results reveal that pH plays an important role in the photocatalytic activity of NiTiO₃. The results for the removal efficiency of RhB pollutant at pH values from 1 to 11 showed a maximum at pH 3.

Graphic abstract



Keywords NiTiO₃ · Visible light · photocatalyst · textile dye

✉ Luong Huu Bac
bac.luonghuu@hust.edu.vn

¹ School of Engineering Physics, Ha Noi University of Science and Technology, No. 1 Dai Co Viet, Ha Noi, Viet Nam

Introduction

Nowadays, visible-light-driven photocatalysts are receiving much attention for wastewater treatment and hydrogen production due to their potential applications in the field of environmental pollution and solar energy conversion.^{1,2} In textile dyeing factories, removal of dyes from wastewater is considered to be an important environmental issue. The presence of dye in wastewater greatly affects animals, plants, and human life.³

Rhodamine B (RhB, C₂₈H₃₁N₂O₃Cl) textile dye, a red-dish-violet powder that is highly water soluble, was used in this work. This dye is a popular colorant and is widely utilized in the garment industry and foodstuffs because it is highly stable.⁴ However, when released into the environment, dyes can be dangerous to aquatic life because they act as toxic, carcinogenic, and mutagenic agents for both humans and animals.⁵ Human beings and animals can be harmed if they swallow released dye in water, and the presence of dye in water can cause irritation to the skin, eyes, and respiratory tract.⁴ Therefore, removal of rhodamine B textile dye from wastewater has become essential for environmental protection. One of the most effective processes to decompose RhB dye is photocatalytic oxidation based on catalytic or chemical photooxidation. This method has emerged as a promising process since Fujishima and Honda reported the evolution of oxygen and hydrogen from a TiO₂ electrode under irradiation of light in 1972⁶ because most pollutants can be completely decomposed to CO₂ and H₂O by using suitable catalysts and irradiation. Photocatalysis is one of the most effective and economical techniques to apply for decoloration of organic textile dyes and solve environmental problems. TiO₂ photocatalyst is the most widely investigated due to its cost-effectiveness, nontoxicity, unique photocatalytic efficiency, and high stability.⁷ The basic mechanism of photocatalytic degradation of pollutants using TiO₂ is related to the absorption of light by the TiO₂ material, which induces charge separation to release electron (e⁻)–hole (h⁺) pairs that result in oxidation–reduction reactions. However, a drawback of pure TiO₂ material is its large bandgap value (3.2 eV for rutile and 3.0 for anatase phase) which limits the application of TiO₂ in practice.^{7–9} Therefore, it is necessary to identify alternative photocatalysts that offer visible-light-driven photocatalytic performance for use in solar energy generation or wastewater treatment.

Nickel titanate is known as a material that exhibit photocatalytic reactivity under visible-light irradiation due to its low bandgap in the range of 2.18 eV to 2.70 eV.^{10,11} Many researchers have investigated the photocatalytic applications of NiTiO₃ under visible-light illumination. Ruiz-Preciado et al. presented the photocatalytic properties of NiTiO₃ thin film for the degradation of Methylene Blue under visible light from a xenon arc lamp.¹⁰ Pugazhenthiran et al. reported the photocatalytic activity of NiTiO₃ rods for degradation of Ceftiofur Sodium under direct sunlight.¹² Hung et al. showed that NiTiO₃ nanopowder decolorated Congo Red under LED visible-light irradiation.¹³ Literature reports indicate that work on the visible-light photocatalytic activity of NiTiO₃ materials has mainly focused on photocatalytic structures and kinds of dyes.^{14,15} However, there is a lack of research on other parameters in practical applications, such as pH, which can also affect the efficiency of the visible-light photocatalytic activity of NiTiO₃ materials. To the best of the

authors' knowledge, no work has reported on the effects of pH on the photocatalytic activity of NiTiO₃ to degrade rhodamine B under visible-light irradiation to date.

The aim of the work described herein is to synthesize NiTiO₃ rods and investigate the effects of the solution pH on the visible light-driven photocatalysis by NiTiO₃ for degradation of RhB textile dye. NiTiO₃ rods were synthesized using an ethylene glycol (EG)-mediated route with ethylene glycol solvent playing the role of a ligand reagent. EG solvent is known to be an effective ligand for metal ions that can create one-dimensional (1D) structures via polymerization of the chain structure. The synthesized NiTiO₃ rods were used for photocatalytic degradation of RhB. The effect of the pH on the removal efficiency of RhB dye was investigated. The results show that adjusting the pH could effectively enhance the photocatalytic properties of the NiTiO₃ rods under visible-light irradiation. A low pH in the dye solution was found to increase the photocatalytic activity of NiTiO₃.

Experimental Procedures

Preparation of NiTiO₃ Rods

Ilmenite NiTiO₃ rods were synthesized by an ethylene glycol-mediated route at room temperature, followed by calcination in air at room temperature. The raw materials were titanium (IV) butoxide [Ti(OC₄H₉)₄], nickel acetate [Ni(CH₃COO)₂·4H₂O], and ethylene glycol. All chemicals used were of analytical grade, obtained from Sigma–Aldrich, and used without further purification. A typical synthesis of NiTiO₃ rods was as follows: 0.01 mol Ni(CH₃COO)₂·4H₂O and 0.01 mol titanium(IV) butoxide [Ti(OC₄H₉)₄] were mixed with 30 mL EG. A light-blue precipitate appeared and increased gradually. After 5 h of stirring, the NiTiO₃ precipitation precursor was collected by centrifuging and washed with deionized water and ethanol for three times then dried under vacuum at 70°C for 6 h. Finally, the powder was calcined for 2 h in air atmosphere to obtain NiTiO₃ rods.

Characterization Techniques

x-Ray diffraction (XRD) patterns were recorded on a Philips X'PertPRO x-ray diffractometer using Ni-filtered Cu K_α radiation at voltage of 40 kV and current of 30 mA in the scan range from 20° to 70°. The crystallite size and micro-strain of the synthesized powders were estimated via the Williamson–Hall method.¹⁶ The morphology of the rods was analyzed by field-emission scanning electron microscopy (Hitachi S4800) equipped with an energy-dispersive x-ray spectroscopy (EDX) system. Diffuse reflectance measurements were performed using a UV–Vis spectrometer

(JASCO V-750) with 60 mm integrating sphere ISV-922. Raman spectroscopy measurements were carried out at room temperature using a micro-Raman spectrometer in combination with a solid-state 633-nm laser as excitation source.

Photocatalytic Degradation Experiments

Photocatalysis experiments were carried out in a cylindrical reactor maintained at 25°C by water circulation. The solution was magnetically stirred continuously throughout the photocatalytic process to ensure sufficient dissolved oxygen in solution. A 50-W white LED lamp was used as visible-light source. The light source was placed on top of the reactor, about 15 cm from the solution, to supply visible light for the reaction. Before illumination, suspension containing 0.04 g photocatalyst and 40 mL RhB solution (5 mg/L) was continuously stirred in the dark for 60 min to attain adsorption–desorption equilibrium of RhB on the surface of the catalyst powder. Samples were taken from the reactor at regular intervals, and the photocatalyst was removed by centrifuging at 5000 rpm for 10 min. The supernatants were analyzed by recording the variations of the absorption band maximum at 553 nm corresponding to the maximum absorption in the UV–Vis spectra using a UV–Vis spectrophotometer (JASCO V-750). The photodegradation ratio was calculated using the equation

$$\text{Degradation rati}(\%) = \frac{C_0 - C}{C_0}, \quad (1)$$

where C_0 is the absorbance of RhB dye before irradiation, and C is the absorbance of RhB at each irradiation time interval. The effect of pH on the photocatalytic activity was investigated by applying different conditions with six pH values of 1, 3, 5, 7, 9, and 11. The pH of the dye solution was adjusted by using 0.1 mol/L HCl or 0.1 mol/L NaOH. The pH level was measured by a commercial pH meter (model HI2020-02).

Results and Discussion

Figure 1 shows the XRD patterns of the synthesized powders after calcination at different temperatures in the range from 500°C to 650°C for 2 h. The sample calcined at 500°C mainly consisted of TiO₂ anatase and NiO phases. At this temperature, almost no NiTiO₃ phase formed. The sample calcined at 550°C presented NiTiO₃ phase formation. However, the impurity phases including rutile TiO₂ (R-TiO₂) and NiO also appeared in this sample. The XRD pattern of the NiTiO₃ annealed at 600°C for 2 h showed high intensity with sharp diffraction peaks, indicating the good crystallinity of the synthesized material. The main diffraction peaks

observed at 2θ values of 24.18°, 33.16°, 35.71°, 40.93°, 49.51°, 54.07°, 57.36°, 62.59°, and 64.21° correspond to (012), (104), (110), (213), (024), (116), (018), (214), and (300) in good agreement with standard Joint Committee on Powder Diffraction Standards (JCPDS) data no. 33–0960 for the rhombohedral crystal structure in space group $R\bar{3}$, confirming that the obtained rods had long-range crystallite structure in pure NiTiO₃ ilmenite phase. No diffraction signals due to any other phases such as NiO, TiO₂, and other related compounds were detected in the XRD spectra, indicating successful synthesis of NiTiO₃ samples. Lattice parameters were estimated by Rietveld refinement. Ilmenite-type NiTiO₃ crystallized in rhombohedral structure with $a = b = 5.0281$ Å, $c = 13.7968$ Å, and cell volume of 302.068 Å³. This XRD result is strongly supported by the Raman spectrum results of NiTiO₃ rods shown in Fig. 2a. Theoretical calculations showed that the optical normal modes of vibrations of NiTiO₃ include ten Raman-active modes: $5A_g(\text{R}) + 5E_g(\text{R})$.^{10,17,18} Ten Raman-active modes $5A_g + 5E_g$ altogether are expected for the prototype phase.¹⁹ In NiTiO₃ materials, the five modes observed at 191.1 cm⁻¹, 246.9 cm⁻¹, 395.2 cm⁻¹, 488.5 cm⁻¹, and 707.6 cm⁻¹ were attributed to A_g symmetry while the five modes seen at 229.5 cm⁻¹, 292.1 cm⁻¹, 347.2 cm⁻¹, 464.8 cm⁻¹, and 612.1 cm⁻¹ were attributed to E_g symmetry.²⁰ The band at 229.5 cm⁻¹ is due to asymmetric vibration of octahedral oxygen. The E_g Raman-active mode bands at 229.5 cm⁻¹, 292.1 cm⁻¹, and 347.2 cm⁻¹ should be governed by the oxygen octahedra, twist of oxygen octahedra, and vibration of Ni and Ti atoms parallel to the xy plane. The A_g Raman band seen at 191.1 cm⁻¹ and 246.9 cm⁻¹ is due to stretching vibration of Ti–O and vibration of Ti along z -axis.²¹ The band located at 612.1 cm⁻¹ is attributed to stretching of Ti–O.²⁰ The highest frequency of 707.6 cm⁻¹ arises from the vibration mode of TiO₆ octahedra.²¹ The ten Raman-active modes observed for the synthesized NiTiO₃ powder confirm its rhombohedral structure, in agreement with literature reports.^{10,20}

Figure 2b shows the EDS analysis of the NiTiO₃ sample calcined at 600°C for 2 h, confirming that the NiTiO₃ rods were composed of Ni, Ti, and O. The detailed composition of the rods from the EDS analysis is summarized in the inset of Fig. 2b, confirming that the composition of the rods accorded with the stoichiometric ratio of NiTiO₃ overall. Therefore, the results described above confirm the formation of pure NiTiO₃ ilmenite phase.

The crystalline size and microstrain of the NiTiO₃ rods were estimated from the broadening of the XRD peaks using the Williamson–Hall method.^{16,22} Microstrain is related to the numbers of defects and crystal imperfections, which include point defects, grain boundaries, dislocations, stacking faults, etc. The line width observed in the XRD spectrum can be simply expressed as the sum of two contributions given by the equation:¹⁶

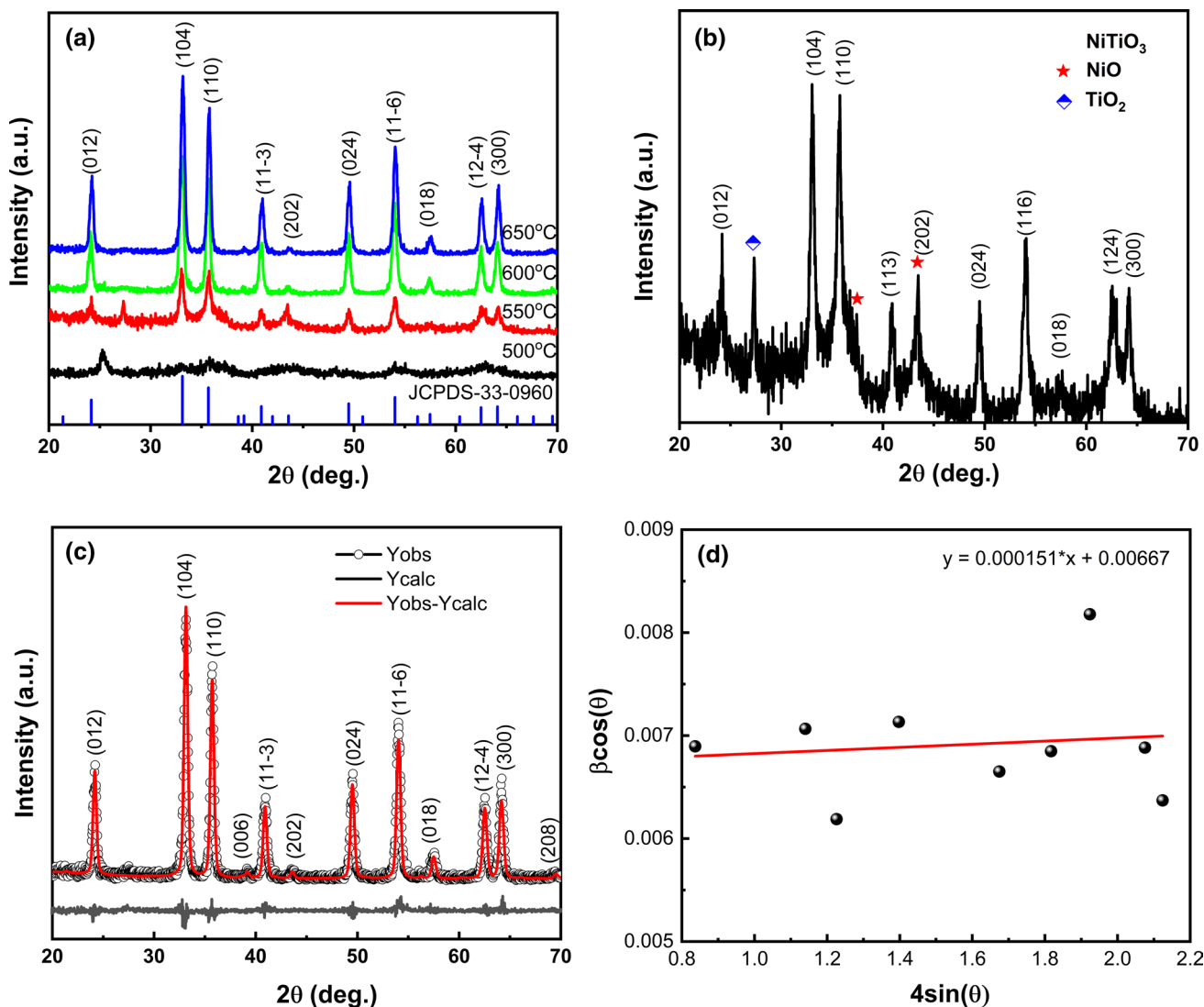


Fig. 1 XRD patterns of (a) NiTiO₃ calcined at different temperatures, (b) magnification of XRD pattern of NiTiO₃ calcined at 550°C, (c) Rietveld refinement, and (d) Williamson–Hall plots of NiTiO₃ calcined at 600°C.

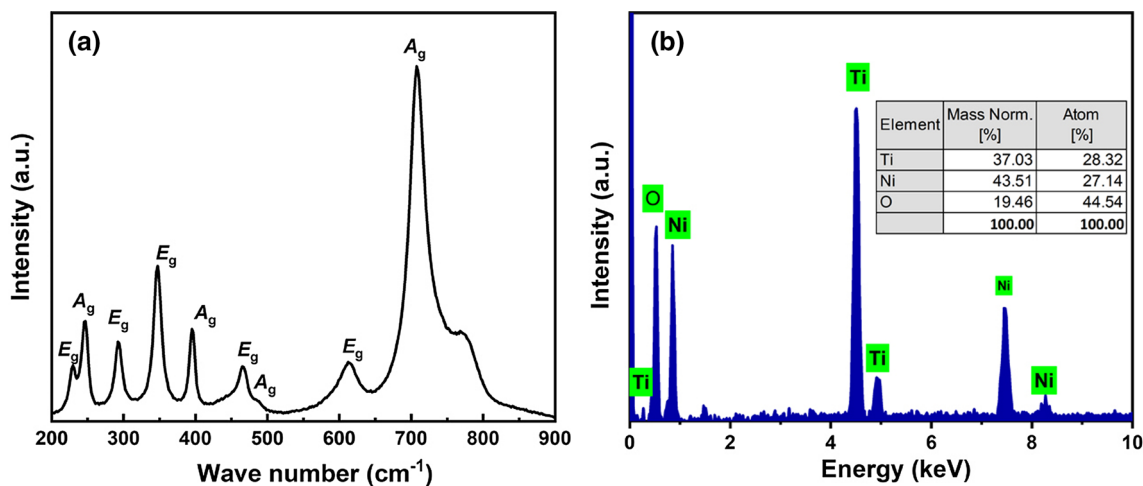


Fig. 2 (a) Raman spectra at room temperature of NiTiO₃ calcined at 600°C and (b) EDX analysis.

$$\beta_r = \frac{k\lambda}{D \cos \theta} + 4 \tan \theta. \quad (2)$$

Rearranging Eq. 2 gives

$$\beta_r \cos \theta = \frac{k\lambda}{D} + 4 \sin \theta, \quad (3)$$

where β_r is the full-width at half-maximum, D is the particle size, and ϵ is the microstrain. The $(k\lambda/D\cos\theta)$ term represents the size broadening, while the $(4\epsilon\tan\theta)$ term represents the microstrain broadening. The microstrain was calculated from the slope of the line, while the crystallite size D was obtained from the intersection with the vertical axis after plotting the dependence of $\beta_r \cos \theta$ versus $4\sin\theta$. Figure 1d shows the Williamson–Hall plot of the NiTiO₃ sample. The average crystallite size and microstrain are 23 nm and 1.5×10^{-4} , respectively. The positive sign of the microstrain indicates lattice expansion of the NiTiO₃ rods. These results

suggest that the synthesized NiTiO₃ rods had nanostructure and contained microstrain. Hence, it can be concluded that pure ilmenite-type rhombohedral phase of NiTiO₃ rods in space group $R\bar{3}$ was successfully synthesized at a minimum temperature of 600°C for 2 h by the ethylene glycol-mediated route.

Figure 3 shows the rod size and surface morphology of the NiTiO₃ rods. The length and diameter of the NiTiO₃ rods were in range from 1.2 μm to 2.3 μm and from 0.1 μm to 0.7 μm , respectively (Fig 3c,d). The rods consisted of many nanoparticles sintered together due to the high annealing temperature (Fig. 3b). The nanoparticles had a roundish shape with average size of around 30 nm. The rods showed a porous structure that could be due to organic residues burned out during calcination at high temperatures.

Figure 4 shows the UV–Vis absorption spectra of the NiTiO₃ rods calcined at different temperatures for 2 h. The NiTiO₃ rods showed two absorption regions in both the UV

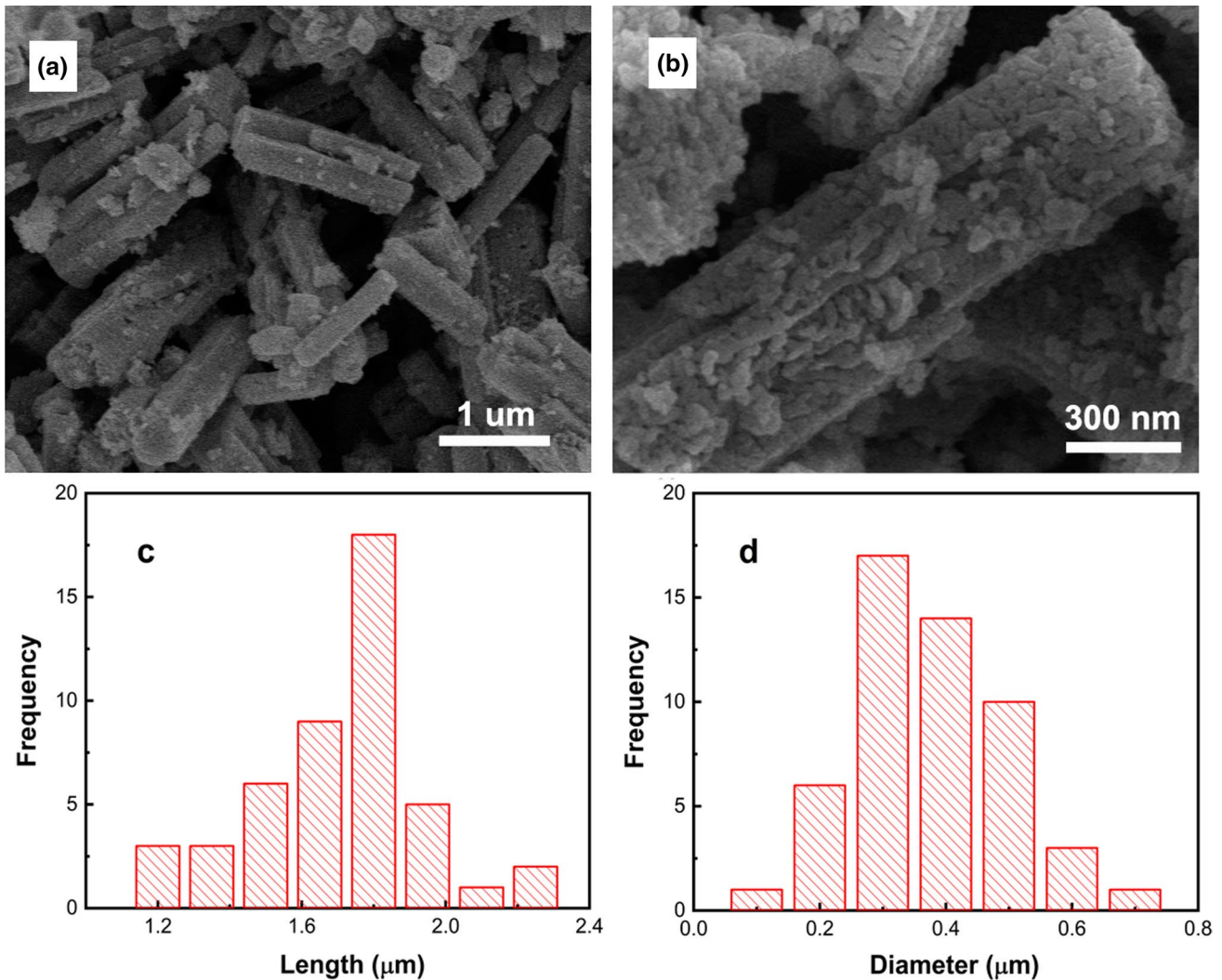


Fig. 3 (a, b) SEM micrographs and (c, d) length and diameter distribution of NiTiO₃ rods calcined at 600°C.

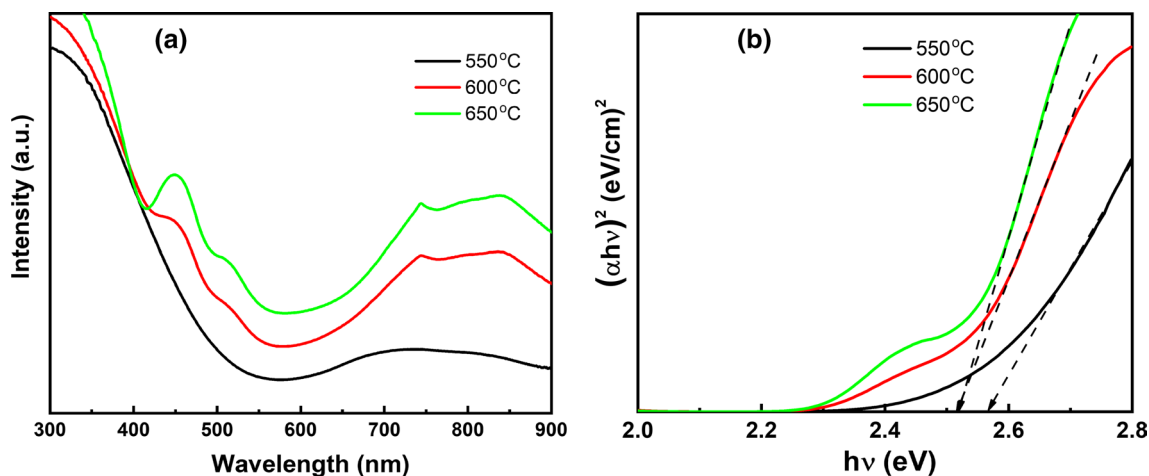


Fig. 4 (a) Optical absorbance spectra and (b) plot of $(\alpha h\nu)^2$ versus photon energy of NiTiO₃ calcined at different temperatures.

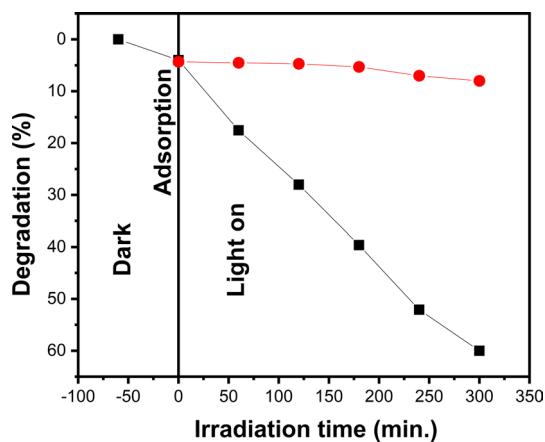


Fig. 5 (a) Photocatalytic degradation efficiency of RhB by NiTiO₃ catalyst under visible-light irradiation.

and visible-light range. The optical bandgap energy was calculated from the Tauc relation from the absorption edge in the near-UV region.²³ The optical bandgap of the synthesized NiTiO₃ calcined at 600°C was about 2.52 eV, and this value remained constant for the NiTiO₃ sample calcined at 650°C. The bandgap of the sample calcined at 550°C was higher (2.57 eV) due to the presence of TiO₂ rutile and NiO impurity phases, as shown in the XRD analysis. These optical bandgap values are consistent with previous studies.¹³ Literature reports show that NiTiO₃ has ilmenite-type structure with an optical bandgap value that depends on the morphology, size, and preparation method.^{20,24,25} The optical absorbance of NiTiO₃ in the visible-light region and the low optical bandgap value of the NiTiO₃ rods make them suitable for visible-light photocatalysis.

Figure 5 shows the RhB degradation efficiency versus the irradiation time of the NiTiO₃ samples under visible-light

irradiation. It is clearly seen that the NiTiO₃ rods could degrade RhB textile dye. The discoloration efficiency in the dark after 1 h is due to the adsorption–desorption equilibrium state which was basically established when the photocatalyst was placed into the dye solution. The degradation efficiency of RhB without NiTiO₃ photocatalyst slowly decreased with irradiation. It was only 7% after the dye solution had been illuminated for 5 h. The dye removal efficiency increased with the presence of NiTiO₃ rods and reached 60%, indicating that NiTiO₃ photocatalyst is efficient for textile dye degradation. NiTiO₃ rods adsorbed the dye on their surface due to their nanostructure and porosity. Under photon excitation from the light irradiation, NiTiO₃ photocatalyst undergoes photon-induced charge separation to produce electron–hole pairs. The hole–electron charges ($h^+_{VB} + e^-_{CB}$) can recombine and dissipate the absorbed optical energy, or migrate to the NiTiO₃ photocatalyst surface and begin a redox reaction with adsorbed RhB dye molecules. The reduction and oxidation process by the photo-excited electrons (e^-_{CB}) and by positive holes (h^+_{VB}) at the photocatalyst surface result in decoloration of the RhB dye via mineralization into nontoxic substances.

Textile industries release wastewater including various contaminants at a wide range of pH values.²⁶ Generally, the pH plays an important role in both the characteristics of textile waste and the generation of hydroxyl radicals. Changing the pH can thus affect the adsorption of dye molecules onto the NTO particle surface, which is one of the important steps for the photocatalytic activity to occur. Therefore, we investigated the role of the solution pH in the photocatalytic degradation of RhB under the determined experimental condition with an initial RhB concentration of 5 mg/L and NTO dose of 1 g/L. The pH of the dye solution was adjusted using sodium hydroxide (NaOH) in the case of alkaline solutions or hydrochloric acid (HCl)

in the case of acidic solutions. Figure 6 shows the effect of pH on the photocatalytic activity of the NiTiO₃ rods. The removal efficiency was investigated at different pH values at constant dye concentration. It is clearly seen that the pH dramatically affected the photocatalytic reaction. The decolorization rate of RhB in acidic media was higher than that in alkaline media. The dye degradation was significantly decreased under the alkaline condition but dramatically increased under the acid condition. The experimental results show that pH 3 was the best condition for RhB degradation, achieving 99% after 3 h under LED visible-light irradiation. Higher pH values resulted in worse degradation, and the dye removal decreased as the pH of the dye solution was increased. The degradation efficiency went down from 99% at pH 3 to only 35% and 14% of RhB after 5 h irradiation at pH 9 and 11, respectively.

The degradation efficiency of RhB dye was strongly influenced by the pH, which can be explained by the variation of the charge on RhB with the pH. Depending on the dye concentration and the pH of the dye solution, RhB dye can be ionized to different degrees because it includes chloride cation and carboxylic acid group.²⁷ Thus, the RhB molecules can assume different net charges depending on the experimental conditions.^{28,29} Mendonça et al. showed that the acid group of RhB dissociated to more than 99% in the basic pH range, enabling the formation of electronically neutral RhB molecules.²⁹ Morín et al. presented that the zeta potential becomes positive when the pH becomes more acidic and the isoelectric point (IEP) of NiTiO₃ materials is 5.7.³⁰ NiTiO₃ has a negative surface charge in alkaline conditions. The resulting weak interaction between NiTiO₃ and RhB molecules in the basic pH

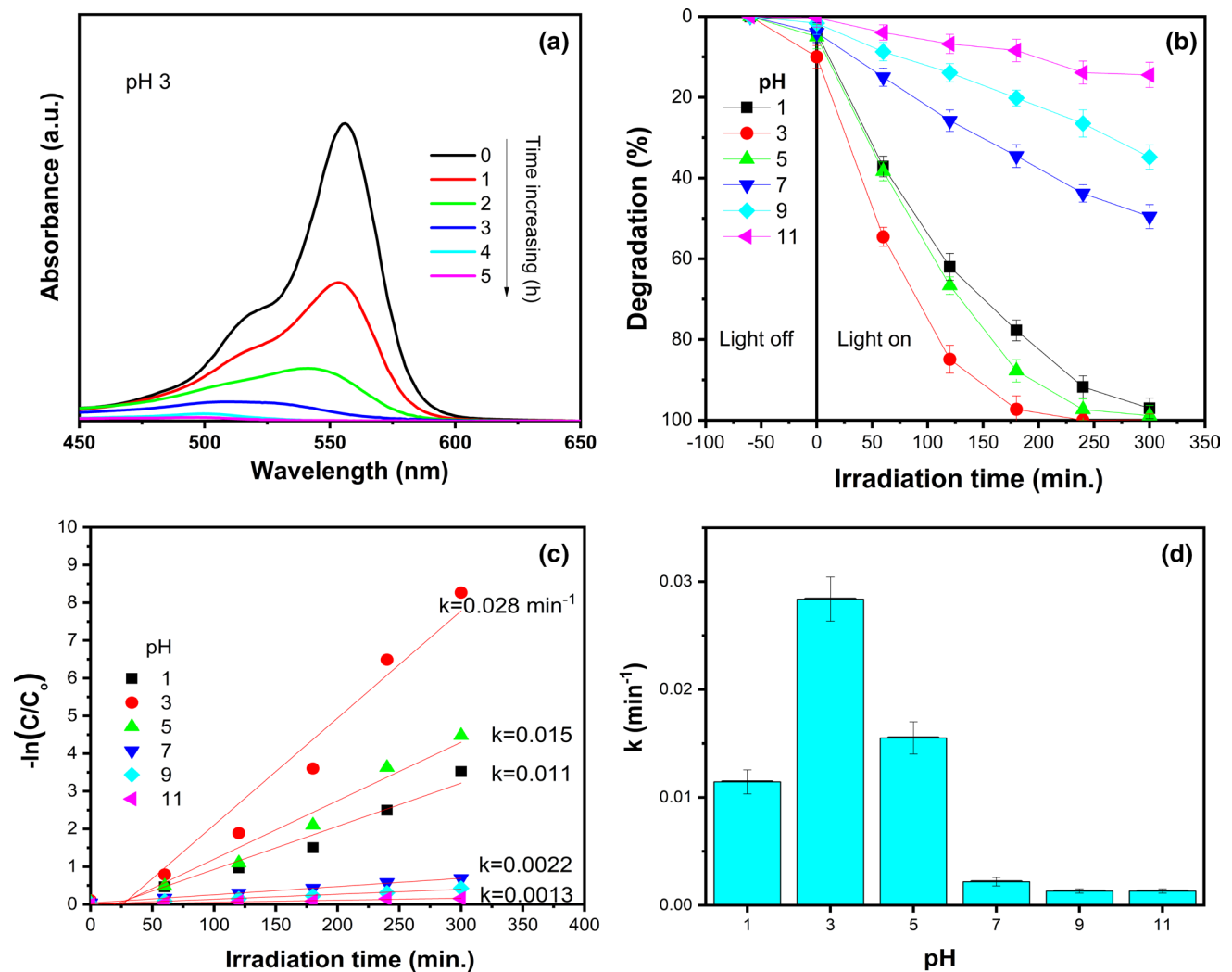
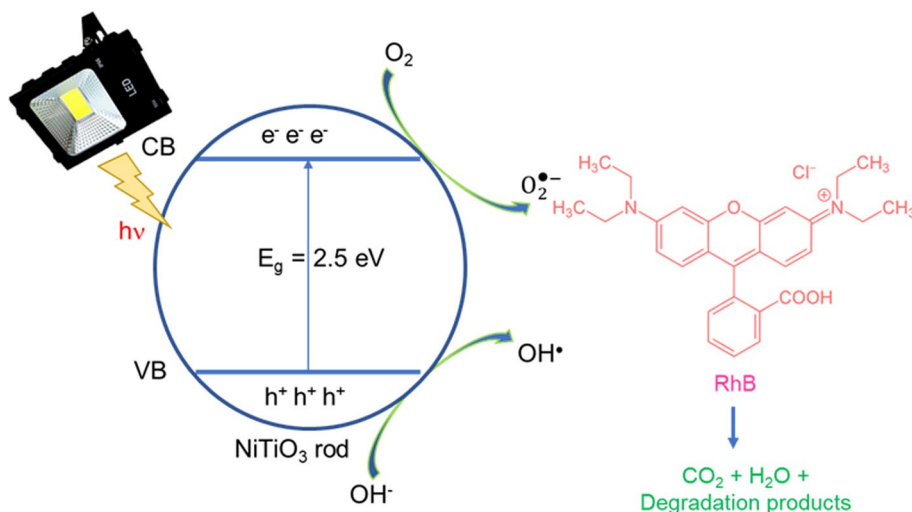


Fig. 6 (a) UV-Vis absorption spectra of RhB after irradiation for various times at pH 3. (b) Photocatalytic degradation efficiency of RhB at different pH values. (c) First-order kinetics plot for photodegradation

of RhB by NiTiO₃ under visible-light irradiation in environments with different pH values, and (d) degradation rate constant k (min⁻¹).

Fig. 7 Photocatalytic mechanism of NiTiO₃ rods under LED visible-light irradiation.



range thus results in a low dye degradation rate. At low pH, the carboxyl group of RhB is negatively charged in acid condition,³¹ resulting in a strong reaction between NiTiO₃ and RhB molecules. This strong interaction could enhance the dye degradation and result in the higher efficiency under acidic than alkaline conditions.

To provide further insight, the degradation kinetics of RhB on the surface of NiTiO₃ catalyst was calculated. The Langmuir–Hinshelwood model was used to investigate the kinetics of the photocatalytic reaction based on the equation³²

$$r = -dC/dt = kKC/(1 + KC), \quad (4)$$

where r is the reaction rate (mol/L/min), C is the equilibrium concentration of reagent (mol/L), t is time (min), k is the rate constant (L/min), and K is the Langmuir constant (L/mol). This equation can be simplified to the following pseudo-first-order expression when the concentration of the reagent that is reacting is very low:³³

$$r = -dC/dt = k_{app}C, \quad (5)$$

where k_{app} is the pseudo-first-order rate constant (min⁻¹).

Integrating Eq. 5 results in

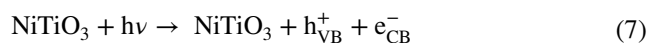
$$-\ln(C_t/C_0) = k_{app}t, \quad (6)$$

where C_t and C_0 are the dye concentration (mol/L) at instants t and $t = 0$, respectively.³⁴

The photocatalytic degradation curves of the NiTiO₃ samples were well fit by pseudo-first-order kinetics, as shown in Fig. 6c. The estimated kinetic constant k is presented in Fig. 6d. The kinetic constants for RhB photodegradation first increased with increase of the pH value, reached a maximum at pH 3, then went down at pH values above 3. On changing the pH value of the solution, the

kinetic constant of NTO reached its maximum value of 0.028 min⁻¹ at pH . These results confirm that dye degradation at low pH efficiently enhanced the photocatalytic capability under visible-light irradiation. The enhanced photocatalytic activity can mainly be ascribed to the dependence of the charges on the RhB molecules and the surface of the NiTiO₃ particles, which enhanced the interaction between them and increased the visible-light absorption on the surface, resulting in high efficiency in acidic environment. In alkaline condition, the kinetic constant was small with a value of only 0.0013 min⁻¹ and 0.0005 min⁻¹ at pH 9 and 11, respectively.

Figure 7 illustrates the photocatalytic mechanism of NiTiO₃ rods under LED visible-light irradiation. The conduction band (CB) and valence band (VB) position of the photocatalyst determine its redox ability. An electron in the VB is excited to the CB (e^-_{CB}), resulting in the formation of a hole in the VB (h^+_{VB}) when the photocatalyst is irradiated by LED visible light. Oxygen adsorbed on the surface of the NiTiO₃ photocatalyst can be reduced by photoexcited electrons in the conduction band to form superoxide radicals ($O_2^{\bullet-}$), and hydroxide and water can be oxidized by h^+ in the valence band to form hydroxyl radicals. These active groups created by the redox processes react with RhB dye molecules and change them into H₂O, CO₂, and/or nontoxic substances. The narrow optical bandgap and surface porosity of NiTiO₃ rods make them suitable as a photocatalyst for textile degradation under visible-light irradiation.





Conclusions

The effect of pH on the photodegradation of RhB textile dye by NiTiO₃ rods was investigated under LED visible-light irradiation. NiTiO₃ rods with porous surface were synthesized in pure ilmenite crystal phase and exhibited visible light-induced photocatalytic degradation of rhodamine B. We show that the photocatalytic activity of NiTiO₃ rods strongly depends on the pH of the aqueous rhodamine B solution and can thus be controlled by adjusting the pH value of the dye solution. This result suggests that NiTiO₃ rods have potential applications for dye degradation under visible-light irradiation.

Acknowledgments This research is funded by Vietnam National Foundation for Science and Technology Development (NAFOSTED) under grant no. 103.02-2020.27.

Conflict of interest The authors declare that they have no conflict of interest.

References

1. S. Dong, J. Feng, M. Fan, Y. Pi, L. Hu, and X. Han, *Recent developments in heterogeneous photocatalytic water treatment using visible light-responsive photocatalysts: a review* *RSC Adv.* 5, 14610–14630 (2015).
2. N. Fajrina, and M. Tahir, *A critical review in strategies to improve photocatalytic water splitting towards hydrogen production* *Int. J. Hydrogen Energy* 44, 540–577 (2018).
3. H. Liu, W. Guo, Y. Li, S. He, and C. He, *Photocatalytic degradation of sixteen organic dyes by TiO₂/WO₃-coated magnetic nanoparticles under simulated visible light and solar light* *J. Environ. Chem. Eng.* 6, 59–67 (2018).
4. R. Jain, M. Mathur, S. Sikarwar, and A. Mittal, *Removal of the hazardous dye rhodamine B through photocatalytic and adsorption treatments* *J. Environ. Manag.* 85, 956–964 (2007).
5. R. Nagaraja, N. Kottam, C.R. Girija, and B.M. Nagabhushana, *Photocatalytic degradation of Rhodamine B dye under UV/solar light using ZnO nanopowder synthesized by solution combustion route* *Powder Technol.* 215–216, 91–97 (2012).
6. A. Fujishima, and K. Honda, *Electrochemical photolysis of water at a semiconductor electrode* *Nature* 238, 37–38 (1972).
7. K. Hashimoto, H. Irie, and A. Fujishima, *TiO₂ photocatalysis: a historical overview and future prospects* *Jpn. J. Appl. Phys.* 44, 8269–8285 (2005).
8. K.M. Reza, A. Kurny, and F. Gulshan, *Parameters affecting the photocatalytic degradation of dyes using TiO₂: a review* *Appl. Water Sci.* 7, 1569–1578 (2017).
9. M.M. Byranvand, A.N. Kharat, L. Fathollahi, and Z.M. Beiranvand, *A review on synthesis of Nano-TiO₂ via different methods* *J. Nanostruct.* 3, 1–9 (2013).
10. M.A. Ruiz-Preciado, A. Bulou, M. Makowska-Janusik, A. Gibaud, A. Morales-Acevedo, and A. Kassiba, *Nickel titanate (NiTiO₃) thin films: RF-sputtering synthesis and investigation of related features for photocatalysis* *CrystEngComm* 18, 3229–3236 (2016).
11. X. Shu, J. He, and D. Chen, *Visible-light-induced photocatalysis based on nickel titanate nanoparticles* *Ind. Eng. Chem. Res.* 2, 4750–4753 (2008).
12. N. Pugazhenthiran, K. Kaviyaran, T. Sivasankar, A. Emeline, D. Bahnemann, R.V. Mangalaraja, and S. Anandan, *Sonochemical synthesis of porous NiTiO₃ nanorods for photocatalytic degradation of ceftiofur sodium* *Ultrason. Sonochem.* 35, 342–350 (2017).
13. P.P. Hung, T.T. Dat, D.D. Dung, N.N. Trung, M.H. Hanh, D.N. Toan, and L.H. Bac, *Effect of annealing temperature on structural, optical and visible-light photocatalytic properties of NiTiO₃ nanopowders* *J. Electron. Mater.* 47, 7301–7308 (2018).
14. Q. Li, Y. Xing, L. Zong, R. Li, and J. Yang, *Nickel titanates hollow shells: nanosphere, nanorod, and their photocatalytic properties* *J. Nanosci. Nanotechnol.* 13, 504–508 (2013).
15. P. Jing, W. Lan, Q. Su, M. Yu, and E. Xie, *Visible-light photocatalytic activity of novel NiTiO₃ nanowires with rosary-like shape* *Sci. Adv. Mater.* 6, 434–440 (2014).
16. A.K. Zak, W.H.A. Majid, M.E. Abrishami, and R. Youse, *X-ray analysis of ZnO nanoparticles by Williamson e Hall and size e strain plot methods* *Solid State Sci.* 13, 251–256 (2011).
17. Y. Fujioka, J. Frantti, A. Puzetzy, and G. King, *Raman study of the structural distortion in the Ni_{1-x}CoxTiO₃ solid solution* *Inorg. Chem.* 55, 9436–9444 (2016).
18. G. Busca, G. Ramis, J.M.G. Amores, V.S. Escibano, and P. Piaggio, *FT Raman and FTIR studies of titanias and metatitanate powders* *J. Chem. Soc. Faraday Trans.* 90, 3181–3190 (1994).
19. Y. Fujioka, J. Frantti, A. Puzetzy, and G. King, *Raman study of the structural distortion in the Ni_{1-x}CoxTiO₃ solid solution* *Inorg. Chem.* 55, 9436–9444 (2016).
20. J.B. Bellam, M.A. Ruiz-Preciado, M. Edely, A.J. Szade, and A.H. Kassiba, *Visible-light photocatalytic activity of nitrogen-doped NiTiO₃ thin films prepared by a co-sputtering process* *R. Soc. Chem.* 5, 10551–10559 (2015).
21. V. Chellasamy, and P. Thangadurai, *Structural and electrochemical investigations of nanostructured NiTiO₃ in acidic environment* *Front. Mater. Sci.* 11, 162–170 (2017).
22. J. Singh, S. Sharma, S. Sharma, and R.C. Singh, *Effect of tungsten doping on structural and optical properties of rutile TiO₂ and band gap narrowing* *Optik* 182, 538–547 (2019).
23. N.T. Hung, N.H. Lam, A.D. Nguyen, L.H. Bac, N.N. Trung, D.D. Dung, Y.S. Kim, N. Tsogbadrakh, T. Ochirkhuyag, and D. Odkhuu, *Intrinsic and tunable ferromagnetism in Bi_{0.5}Na_{0.5}TiO₃ through CaFeO₃-δ modification* *Sci. Rep.* 10, 1–15 (2020).
24. P. Yuan, C. Fan, G. Ding, Y. Wang, and X. Zhang, *Preparation and photocatalytic properties of ilmenite NiTiO₃ powders for degradation of humic acid in water* *Int. J. Miner. Metall. Mater.* 19, 372–376 (2012).
25. M.A. Ruiz-Preciado, A. Kassiba, A. Gibaud, and A. Morales-Acevedo, *Comparison of nickel titanate (NiTiO₃) powders synthesized by sol-gel and solid state reaction* *Mater. Sci. Semicond. Process.* 37, 171–178 (2015).
26. N. Bouanimba, N. Laid, R. Zouaghi, and T. Sehili, *Effect of pH and inorganic salts on the photocatalytic decolorization of methyl orange in the presence of TiO₂ P25 and PC500* *Desalin. Water Treat.* 53, 1–13 (2013).

27. H.A.J.L. Mourão, O.F. Lopes, C. Ribeiro, and V.R. Mastelaro, *Rapid hydrothermal synthesis and pH-dependent photocatalysis of strontium titanate microspheres Mater. Sci. Semicond. Process.* 30, 651–657 (2015).
28. X. Zhang, J. Yao, D. Li, X. Chen, H. Wang, L.Y. Yeo, and J.R. Friend, *Self-assembled highly crystalline TiO₂ mesostructures for sunlight-driven, pH-responsive photodegradation of dyes Mater. Res. Bull.* 55, 13–18 (2014).
29. P. Process, S. Paulo, and S. Paulo, *The role of the relative dye-photocatalyst concentration in TiO₂ assisted photodegradation process Photochem. Photobiol.* 90, 66–72 (2014).
30. E. Zaraz, L. Torres-mart, D. Sanchez-mart, N. Le, S. Nicol, and G.N. Le, *Photocatalytic performance of titanates with formula MTiO₃ (M = Fe, Ni, and Co) synthesized by solvo-combustion method Mater. Res.* 20, 1322–1331 (2017).
31. F. Chen, J. Zhao, and H. Hidaka, *Highly selective deethylation of rhodamine B: adsorption and photooxidation pathways of the dye on the TiO₂/SiO₂ composite photocatalyst Int. J. Photoenergy* 05, 2003–2017 (2003).
32. J. Li, Y. Liu, H. Li, and C. Chen, *Fabrication of g-C₃N₄/TiO₂ composite photocatalyst with extended absorption wavelength range and enhanced photocatalytic performance J. Photochem. Photobiol. A* 317, 151–160 (2016).
33. J.M. Herrmann, *Heterogeneous photocatalysis: fundamentals and applications to the removal of various types of aqueous pollutants Catal. Today* 53, 115–129 (1999).
34. M. Hosseini-Zori, *Co-doped TiO₂ nanostructures as a strong antibacterial agent and self-cleaning cover: synthesis, characterization and investigation of photocatalytic activity under UV irradiation J. Photochem. Photobiol., B* 178, 512–520 (2018).

Publisher's Note Springer Nature remains neutral with regard to jurisdictional claims in published maps and institutional affiliations.